METHOD

Template switching enables chemical probing of native RNA structures

IAN HALL,[1,4] MARTIN O'STEEN,[2,4] SOPHIE GOLD,[1] SARAH C. KEANE,[1,2] and CHASE A. WEIDMANN[3]

[1]Department of Chemistry, University of Michigan, Ann Arbor, Michigan 48109, USA

[2]Program in Biophysics, University of Michigan, Ann Arbor, Michigan 48109, USA

[3]Department of Biological Chemistry, Center for RNA Biomedicine, Rogel Cancer Center, University of Michigan Medical School, Ann Arbor, Michigan 48109, USA

ABSTRACT

RNAs are often studied in nonnative sequence contexts to facilitate structural studies. However, seemingly innocuous changes to an RNA sequence may perturb the native structure and generate inaccurate or ambiguous structural models. To facilitate the investigation of native RNA secondary structure by selective 2′ hydroxyl acylation analyzed by primer extension (SHAPE), we engineered an approach that couples minimal enzymatic steps to RNA chemical probing and mutational profiling (MaP) reverse transcription (RT) methods—a process we call template switching and mutational profiling (Switch-MaP). In Switch-MaP, RT templates and additional library sequences are added postprobing through ligation and template switching, capturing reactivities for every nucleotide. For a candidate SAM-I riboswitch, we compared RNA structure models generated by the Switch-MaP approach to those of traditional primer-based MaP, including RNAs with or without appended structure cassettes. Primer-based MaP masked reactivity data in the 5′ and 3′ ends of the RNA, producing ambiguous ensembles inconsistent with the conserved SAM-I riboswitch secondary structure. Structure cassettes enabled unambiguous modeling of an aptamer-only construct but introduced nonnative interactions in the full-length riboswitch. In contrast, Switch-MaP provided reactivity data for all nucleotides in each RNA and enabled unambiguous modeling of secondary structure, consistent with the conserved SAM-I fold. Switch-MaP is a straightforward alternative approach to primer-based and cassette-based chemical probing methods that precludes primer masking and the formation of alternative secondary structures due to nonnative sequence elements.

Keywords: SHAPE; MaP-RT; native RNA structure; riboswitch

INTRODUCTION

In recent decades, the discovery of functional noncoding (nc) RNAs has increased exponentially (Reinhart et al. 2000; Eddy 2001; Lagos-Quintana et al. 2001; Lau et al. 2001; Lee and Ambros 2001; Wassarman et al. 2001; Vogel et al. 2003; Kawano et al. 2005; Mattick and Makunin 2006; Tian et al. 2010; Cech and Steitz 2014; Santosh et al. 2014; Mattick et al. 2023). However, the structural characterization of ncRNA elements—an important step in gaining mechanistic insight to their function—has not kept pace with their rapid discovery. Many structural biology methods have been employed to characterize RNA secondary and/or tertiary structure: including X-ray crystallography, nuclear magnetic resonance (NMR) spectroscopy, chemical probing, small-angle X-ray scattering, and cryo-electron microscopy. X-ray crystallography and NMR spectroscopy in particular have provided gold-standard atomic-resolution 3D models and critical insights into the structure/function relationship of numerous RNAs (Edwards and Ferré-D'Amaré 2006; Thore et al. 2006; Dann et al. 2007; Garst et al. 2008; Assmann et al. 2023).

In contrast, chemical probing approaches like selective 2′ hydroxyl acylation analyzed by primer extension (SHAPE) and mutational profiling (MaP), while currently unable to generate atomic-resolution 3D models alone, provide accurate and nucleotide-level resolution information on secondary and tertiary RNA structure features, including for long RNAs in solution and natively inside cells (Siegfried et al. 2014; Dethoff et al. 2018; Christy et al. 2021; Przanowska et al. 2022). Many MaP experiments

[4]These authors contributed equally to this work.

Corresponding authors: cweidman@umich.edu, sckeane@umich.edu

Handling editor: Adrian Ferre-D'Amare

Article is online at http://www.rnajournal.org/cgi/doi/10.1261/rna.079926.123. Freely available online through the *RNA* Open Access option.

lack reactivity data from 5′ and 3′ ends of an RNA, due to the use of primers during reverse transcription (RT) and polymerase chain reaction (PCR) steps that mask mutations in these regions. Because MaP RT enzymes extend a DNA primer complementary to the 3′ end of an RNA template, modifications within that 3′ sequence will not be captured in the cDNA product. Because this region cannot contain any mutational information, no reactivity data can be recovered. The RT primer may also anneal differently to RNA molecules depending on their level of modification in the primer-binding site, potentially masking the detection of structural variants with unique reactivity in the primer-binding site. Primer masking also occurs during cDNA amplification, where mutations and/or deletions in both forward and reverse primer-binding regions are not transferred into the PCR products.

Strategies to overcome primer masking include postmodification ligations or premodification inclusion of structure cassettes. Ligation approaches—including sequential 3′ and 5′ ligations to modified RNA directly (Maguire et al. 2020) or cDNA circularization following RT from a ligated 3′ adapter (Loughrey et al. 2014; Yamagami et al. 2022)—can effectively capture probing information for all nucleotides within an RNA. However, ligation approaches involve multiple enzymatic steps, require significant RNA input, and can involve multiple gel extractions and purifications. Alternatively, the inclusion of "structure cassettes" flanking an RNA structure of interest streamlines data acquisition by enabling RT and PCR of modified RNA directly (Merino et al. 2005; Wilkinson et al. 2006). Cassettes are typically small, structured hairpins that are presumed to fold independently and not alter the structure of the RNA of interest. These cassettes serve as primer-binding sites for RT and downstream cDNA library preparation, eliminating the loss of mutational data in the RNA of interest due to primer masking. However, addition of nonnative sequence elements may perturb the native RNA fold and lead to inaccurate structural models.

To overcome the limitations of existing technologies, we developed an approach that enables direct chemical probing of an RNA and limits additional preparatory steps while retaining reactivity data for all nucleotides. Our new Switch-MaP approach (template switching mutational profiling) relies on a single RNA ligation step to append a 3′ sequence (Loughrey et al. 2014) and template switching (Zhu et al. 2001) during MaP RT to append the 5′ sequence. Like sequential ligation methods, Switch-MaP adds all additional sequences necessary for analysis after chemical probing of an RNA in a native sequence context. The major innovation of Switch-MaP is the use of template switching to incorporate 5′ sequences during MaP RT, eliminating downstream enzymatic steps present in existing protocols. This new library design approach generates cDNA products that can be amplified with PCR primers that do not mask probed RNA sequences, enabling full-length readout of chemical probing information from native sequence contexts.

We validated Switch-MaP by experimentally determining the SHAPE-informed secondary structure of a candidate *S*-adenosylmethionine (SAM) class I riboswitch. We compared models derived from both primer-masked and structure cassette MaP experiments to those generated from Switch-MaP. SAM-I riboswitch aptamer domain secondary and tertiary structures have been extensively characterized and represent an excellent model system for the validation of our MaP method (Winkler et al. 2003; McDaniel et al. 2005; Fuchs et al. 2006; Montange and Batey 2006; Lu et al. 2010 ; Montange et al. 2010; Stoddard et al. 2010; Schroeder et al. 2011). SAM riboswitch element A (*SreA*) was identified as a candidate SAM-I riboswitch in the *Listeria monocytogenes* EGD-e genome (Toledo-Arana et al. 2009). The SreA aptamer domain has high sequence conservation with the SAM-I riboswitch family and is expected to fold into a four-way helical junction with helices P1–P4 and junctions J1/2, J2/3, J3/4, and J4/1 (Batey 2011). Limited structure is expected in the 5′ leader sequence of the full-length riboswitch, while the expression platform downstream from the aptamer domain is anticipated to sample mutually exclusive "terminator" (transcription OFF) and "antiterminator" (transcription ON) conformations. We applied Switch-MaP to full-length and aptamer domain SreA RNA constructs and found that Switch-MaP-derived reactivities permitted accurate and unambiguous modeling of highly conserved features of the SreA riboswitch. Access to reactivity information for all nucleotides was essential for accurate prediction of P2, P3, and J3/4 and correct assignment of terminator/antiterminator conformation. In contrast, data from primer-masked or structure cassette constructs supported either incorrect or ambiguous structure models.

RESULTS

Issues with incomplete and nonnative MaP data

The interest in developing Switch-MaP came from attempts to chemically probe the structure of the candidate SAM-I riboswitch SreA. We probed a variety of SreA RNA constructs in solution with the well-established SHAPE reagent 1-methyl-7-nitroisatoic anhydride (1M7) or, as a background control, DMSO. We prepared both native RNA constructs and RNA constructs that include 5′ and 3′ structure cassettes, with variants including the SreA riboswitch or only the ligand-binding aptamer domain. RNA was transcribed from a DNA template by T7 RNA polymerase, purified, and folded in solution before chemical probing, and modified RNAs were used to prepare MaP libraries (Fig. 1).

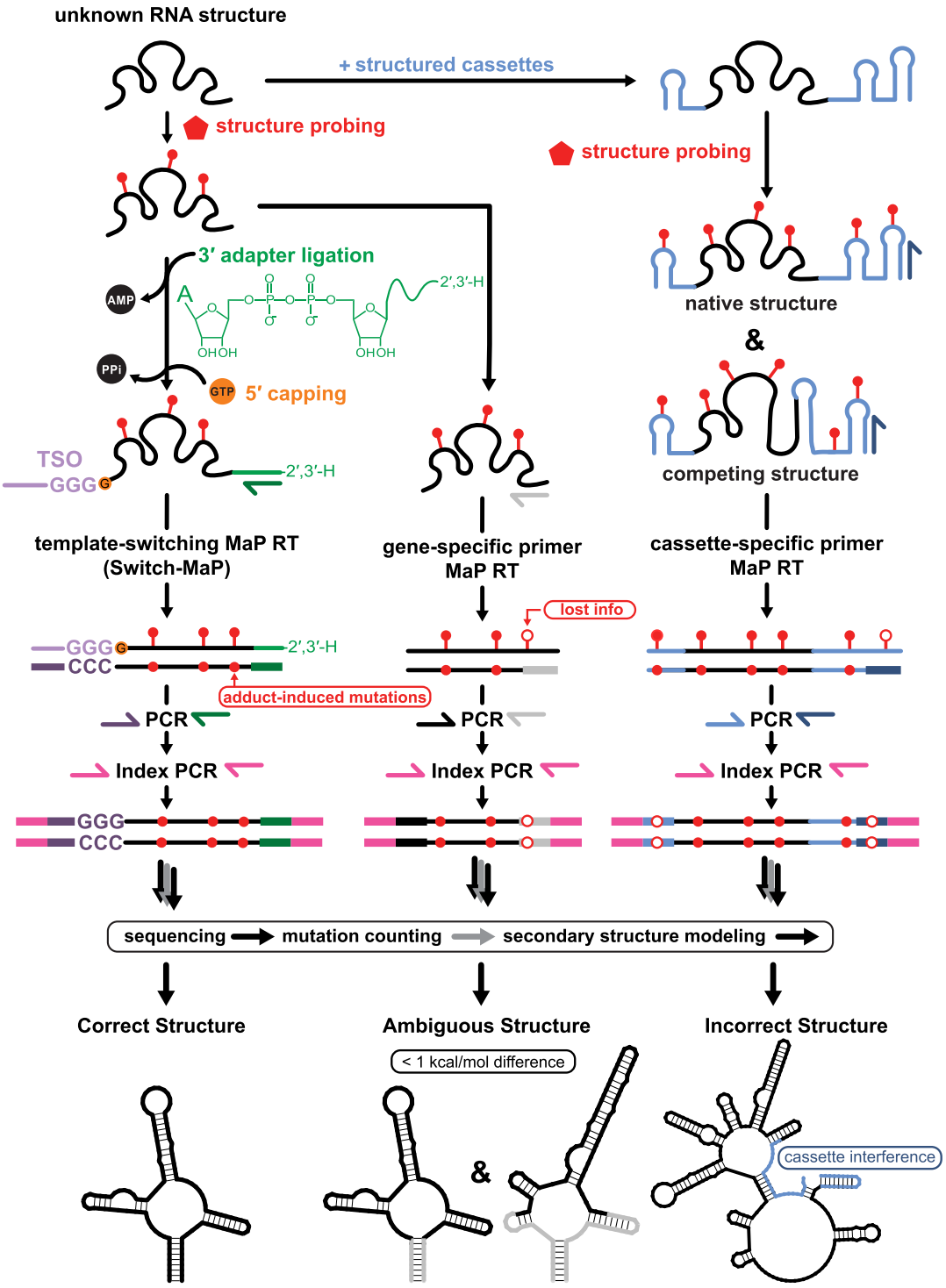

FIGURE 1. Schematic comparison of SreA MaP approaches. A schematic comparing the proposed Switch-MaP approach (*left*) with traditional primer-based (*center*) and cassette-MaP (*right*). SHAPE reagent and SHAPE-acylated nucleotides are indicated by red pentagons and circles, respectively. In the Switch-MaP approach, the RT primer-binding site is added postprobing via ligation of a 5′-5′ adenylated oligo containing a dideoxy (H) 3′ terminal nucleotide (green). Subsequent G-capping (orange) supports template switching with a template-switching oligo (TSO, violet) during the MaP RT step. Post-RT, the resulting cDNA is amplified with primers specific for these appended sequences, preserving reactivity information in the native sequence. Indexing PCR, generating the sequencing library, results in full capture of nucleotide reactivities for the native RNA producing an accurate and unambiguous structure model. In comparison, primer-based MaP approaches lose reactivity information due to primer masking on the 5′ and 3′ ends of the modified RNA (indicated by open circles). This information loss introduces ambiguity in the resulting structural models. The use of structured cassettes (*right*) provides sequence handles for downstream processing but may introduce non-native structure to the RNA of interest (cassette interference).

Direct MaP of 1M7 probed SreA yields incorrect and ambiguous structure models

We first acquired SHAPE reactivities from MaP RT and PCR of the 1M7-modified SreA aptamer domain using primers complementary to the 5′ and 3′ ends. Primers are incorporated directly into cDNA libraries, meaning their sequences carry no modifications and prevent acquisition of reactivity data from complementary sequences on the RNA. We measured the SHAPE reactivities of the remaining aptamer domain nucleotides—which do not include primer-binding sites—and used these as added restraints in RNAStructure (Deigan et al. 2009; Reuter and Mathews 2010; Hajdin et al. 2013; Busan and Weeks 2018) to model secondary structure (Fig. 2; Supplemental Fig. S3). This approach yielded two structure models with similar SHAPE-informed pseudo-free energies: one resembled the expected structure (Fig. 2, left), and the other included a bifurcated P2 stem and an extended P3 stem (Fig. 2, right). Because the major differences between the structures include alternative pairings within the primer-binding regions, it was not possible to assert from this data alone whether one of the structures was correct or if these conformations are representative of a meaningful dynamic ensemble.

We also modeled the secondary structure of the full-length SreA riboswitch (including the native 5′ leader sequence and expression platform) from a primer-based SHAPE-MaP (Fig. 3). In this experiment, regions complementary to the MaP RT and PCR primers were outside of the aptamer domain but included 5′ leader and 3′ expression platform sequences (Supplemental Table S4). Again, the minimum free energy model was inconsistent with the highly conserved SAM-I riboswitch aptamer domain secondary structure. Without reactivity data for primer-masked nucleotides, structure modeling favored the formation of an antiterminator hairpin and disruption of P1 and P2 (Fig. 3A). The modeled structure was not consistent with either expected conformation of the riboswitch. Instead, this model likely results from the absence of reactivity data for 3′ nucleotides. Low SHAPE reactivity at +45A to +55C would favor their inclusion in the terminator stem (OFF state), while high SHAPE reactivity at +45A to +62U would favor the formation of P2 while conserving formation of the antiterminator (ON state). To test this hypothesis, we simulated reactivity data for nucleotides that were

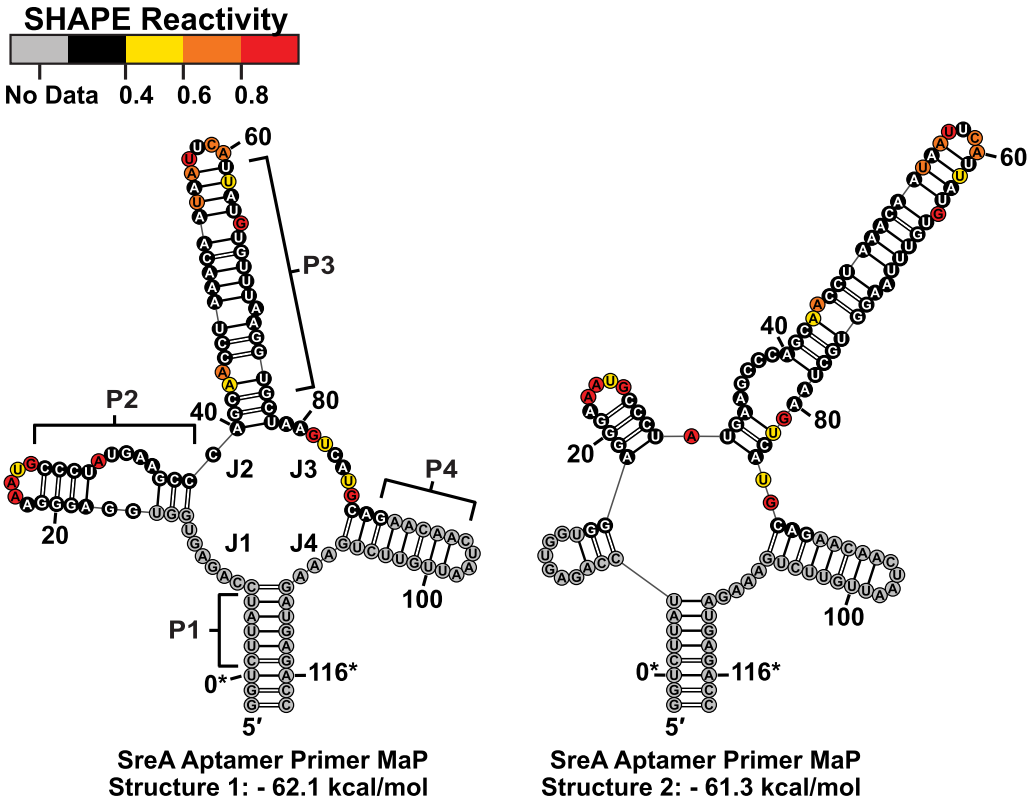

FIGURE 2. Primer-based SHAPE-MaP informed secondary structure of the SreA aptamer. Primer-based MaP of the SHAPE modified of the SreA Aptamer construct produced two competing models with comparable pseudo-free energies. Structure 1 (*left*) is consistent with the expected SAM-I riboswitch aptamer domain secondary structure, containing a four-way junction with well-folded P1–4 helices. Structure 2 (*right*) is characterized by an elongated P3 helix that incorporates portions of the P2 helix and adjacent junction. Secondary structures are numbered based on the native SreA Aptamer domain (nt 0–116).

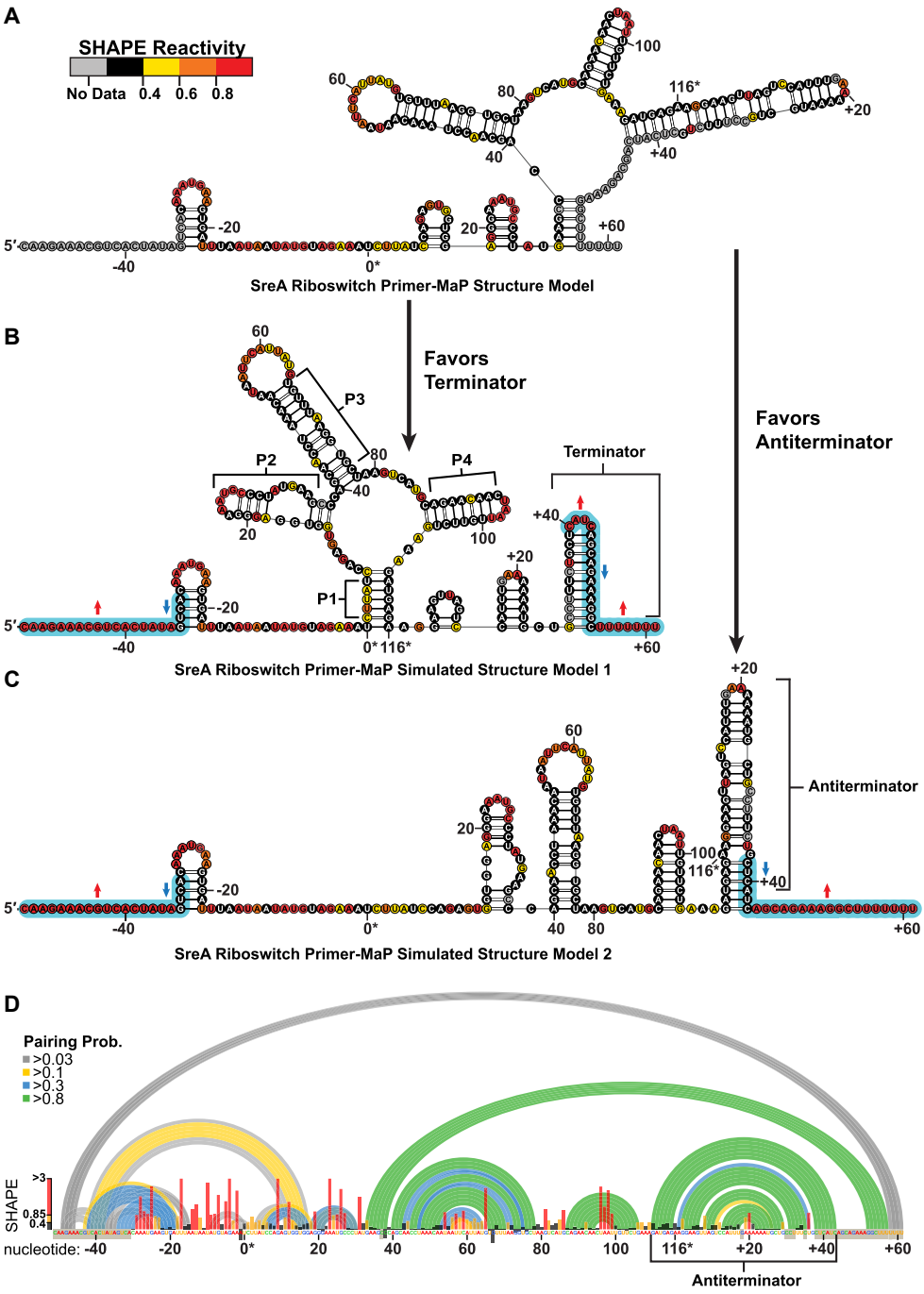

FIGURE 3. Primer-MaP informed secondary structure model of the full-length SreA riboswitch. (*A*) The secondary structure model generated from primer-based MaP revealed a structure incongruent with the expected SAM-I fold due to the loss of reactivity in the 3′ end from primer masking. (*B*,*C*) Simulated reactivity data, indicated by the blue highlights, generate expected terminator (*B*) or antiterminator (*C*) conformations by modeling. (*D*) The pairing probabilities (colored arcs) of the SreA riboswitch derived from SHAPE-informed partition function. Normalized SHAPE reactivities are plotted (bar graph) per nucleotide, along with primer masked or high background sites (gray boxes over nucleotides). The antiterminator helix is the predominant fold in the structural ensemble, nt 110 to +43. Numbering is oriented to the native aptamer sequence (nt 0–116).

masked by either 5′ or 3′ primers to favor the formation the terminator stem (Fig. 3B) or antiterminator stem (Fig. 3C). Manual inspection of SHAPE reactivities supported either conformation (Fig. 3B,C), while the majority of structures present in an ensemble derived from a SHAPE-informed partition function (RNAStructure Suite) (Matthews 2004) included the antiterminator stem (Fig. 3D). As with the aptamer-only construct, we were left with an ambiguous

structure model when relying on primer binding within the target sequence.

Structure cassettes can interfere with native RNA structures

Next, we engineered full-length and aptamer constructs that included extended structure cassettes. These extended sequences serve as primer-binding sites for library construction, allowing the capture of full reactivity data for the target RNA. If the structure cassettes do not interfere with the native RNA structure, this approach can provide reactivity information for all nucleotides within an RNA target along with an internal control for SHAPE reactivity from included cassette helices. Indeed, 1M7 probing of an SreA aptamer construct including structure

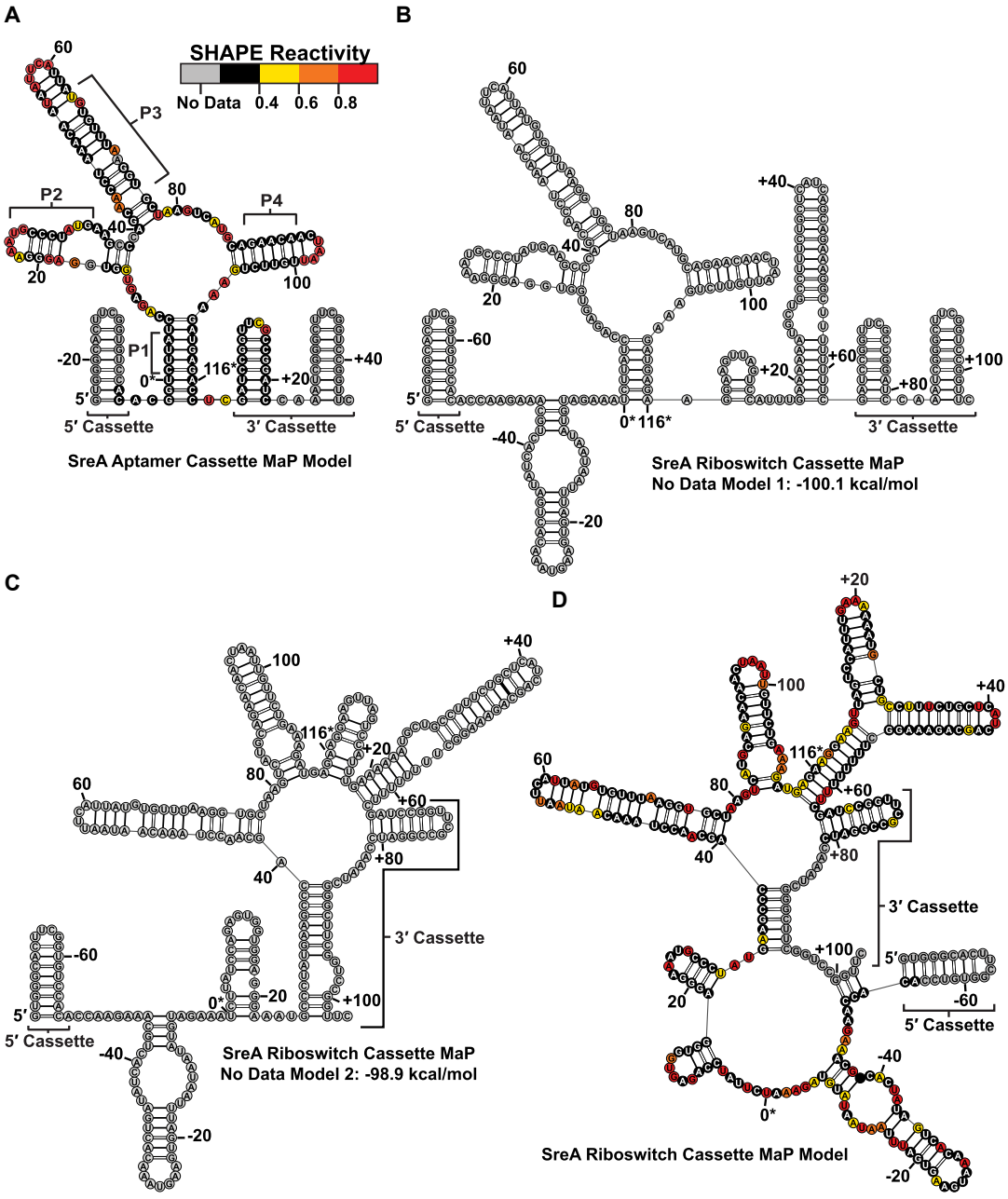

FIGURE 4. Structure models of SreA aptamer and riboswitch including structure cassettes. (*A*) SHAPE-informed secondary structure of the SreA aptamer with flanking structure cassettes, including expected four-way junction structure and P1–4 helices characteristic of SAM-I riboswitches. (*B*) SHAPE data-independent model of the SreA riboswitch with included structure cassettes and (*C*) equivalent energy model including pairing with 3′ structure cassette. (*D*) The SHAPE-informed secondary structure model of the cassette-containing SreA riboswitch includes unintended base pairs with a structure cassette and yielded a model incongruent with SAM-1 riboswitches.

cassettes yielded an unambiguous structure model that agreed with the expected aptamer conformation (Fig. 4A; Supplemental Fig. S4).

However, the SreA riboswitch suffered from incorrect modeling when structure cassettes were included. Without SHAPE data, structure modeling of this construct yielded two structures with comparable free energies; an expected structure, including an antiterminator stem (Fig. 4B), and an incorrect structure, where the 3′ structure cassette base-paired with P2 (Fig. 4C). When 1M7 SHAPE reactivities were included in the structure modeling, minimum free energy models (and the majority of modeled structures) included nonnative pairing between P2 and the 3′ structure cassette (Fig. 4D; Supplemental Fig. S5). While structure cassettes can retain full reactivity information, unintended sequence interactions may perturb the RNA structure.

The failures of primer-masked and structure cassette approaches necessitated the development of a broadly applicable alternative approach to acquire full-length probing information. To address these limitations, we developed the Switch-MaP strategy.

The Switch-MaP strategy

3′ adapter ligation

In the first step of a Switch-MaP library preparation, the 3′ ends of modified RNA (1M7-treated) and unmodified RNA (DMSO-treated) are ligated to a DNA adapter with important features: (1) a 5′-5′ linked adenylate diphosphate (5′-App), obviating the need for ATP during ligation that would otherwise permit RNA–RNA ligation, (2) seven random nucleotides that serve as both a unique molecular identifier and increase sequence diversity during Illumina cluster generation, (3) additional sequence important for Illumina library generation, and (4), a 3′ dideoxy terminal nucleotide that prevents concatemerization of the adapter during ligation (Fig. 1, Switch-MaP workflow) (Supplemental Table S1). The adapter sequence serves as the binding site for RT initiation, acts as a sequence handle for downstream library amplification, and is a standard addition in existing workflows (Loughrey et al. 2014).

5′ capping

After adapter ligation, a guanylate cap (G_{cap}) is added enzymatically to the 5′ end of the RNA to enhance template switching activity of the RT enzyme (Wulf et al. 2022). The G_{cap}—in this work added by the Vaccinia Capping System capable of m^7G cap methylation—is intentionally not methylated during the capping reaction to maximize template switching activity (Wulf et al. 2022). The capping step is potentially omittable, as a variety of 5′ ends are capable of initiating template switching. However, yield of the template-switching step is enhanced by—and in the case of RNAs with a 5′ U nucleotide, dependent—on the presence of a cap structure (Wulf et al. 2022). Adapter-ligated and G-capped RNA serves as a template for MaP RT with SuperScript II enzyme (SSIIRT), with a DNA oligonucleotide complementary to the 3′ adapter serving as the RT primer.

Coupled template switching and mutational profiling RT

SSIIRT enzyme is capable of both MaP RT, where nontemplated nucleotides are added into cDNA product at the site of RNA modifications, and template switching, which enables the extension of cDNA beyond the end of an initial RNA template when a template-switching oligonucleotide (TSO) is provided (Fig. 1, Switch-MaP workflow) (Zhu et al. 2001). Our TSO is a chimeric DNA/RNA oligonucleotide containing specific critical features: (1) a 5′ 5-methyl isodeoxycytosine nucleotide that limits further template switching beyond one TSO, (2) sequence important for Illumina library generation, (3) seven random nucleotides that serve as both a unique molecular identifier and increase sequence diversity during Illumina cluster generation, and (4) three 3′ guanosine ribonucleotides (rG) that anneal to nontemplated cytosine nucleotides added by SSIIRT to the 3′ end of cDNA (Supplemental Table S1). The result of successful template switching is a continuous cDNA product that includes sequences antisense to the 3′ adapter, the full-length RNA, and the TSO. When performed under MaP RT conditions (substituting manganese for magnesium in the buffer, see Methods), the cDNA sequence antisense to the original RNA contains deletions and nontemplated nucleotides (mutations) at sites corresponding to chemically modified RNA nucleotides. This cDNA product can be amplified with standard barcoding primers in preparation for Illumina sequencing while preserving all mutation information in the RNA sequence of interest (Fig. 1, Switch-MaP workflow).

Switch-MaP structure models provide unambiguous information

We modeled the secondary structure of the SreA aptamer and full-length riboswitch from 1M7 probed RNA and Switch-MaP generated libraries (Fig. 5A). For our aptamer-only construct, modeling yielded a single unambiguous minimum free energy model consistent with the conserved SAM-I riboswitch aptamer domain (Fig. 5A, left; Reuter and Mathews 2010). P1–P4 were predicted to fold and were arranged in the anticipated four-way junction with only small differences in the structure of the P3 and the P4 apical loop. Switch-MaP of the full-length SreA riboswitch yielded three similar pseudo-free energy models that support terminator stem formation (Fig. 5A, right, 5B). Formation of the terminator stem was supported by a partition function calculation, where the terminator

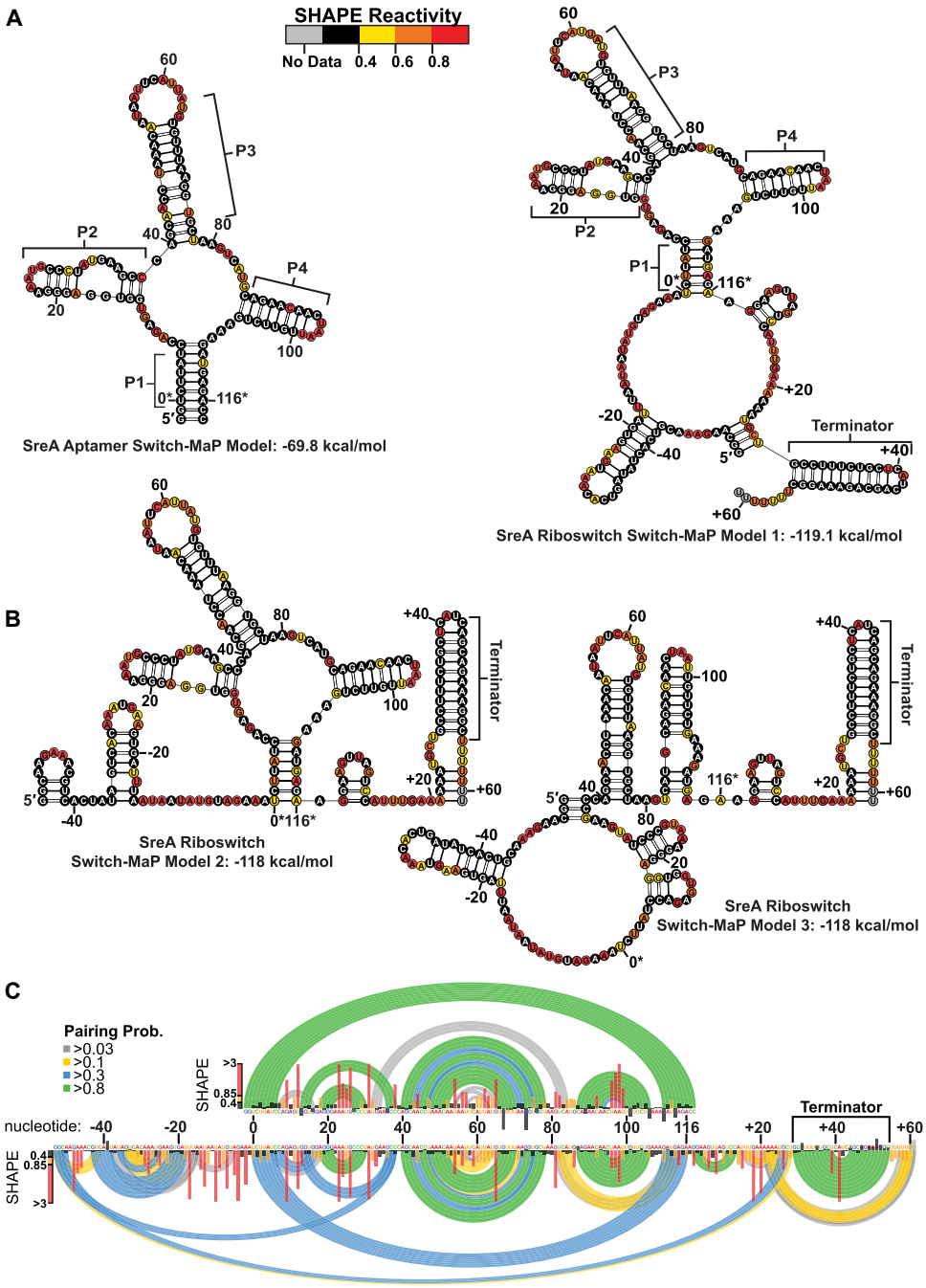

FIGURE 5. Switch-MaP models of the SreA aptamer and full-length SreA riboswitch. (*A*) Switch-MaP SHAPE-informed secondary structures of the SreA aptamer (*left*) and full-length SreA riboswitch (*right*). P1–4 helices of the expected four-way junction are labeled. In the full-length construct (*right*), the expression platform is modeled with a terminator helix. (*B*) Similar pseudo-free energy alternative models of SreA full-length RNA. (*C*) Pairing probability arc plots of aptamer (*top*) and riboswitch (*bottom*) generated from Switch-MaP. The riboswitch plot is inverted and manually aligned to the aptamer plot. Normalized SHAPE reactivities are also plotted as colored bars for every nucleotide. Two 3′ terminal U nucleotides of the riboswitch are grayed out due to high background mutation rates (common during MaP of homopolymeric regions like this one).

stem was present in more than 80% of the modeled structural ensemble (Fig. 5C). For the full-length SreA riboswitch, Models 1 and 2 (Fig. 5A, right, 5B, left) also support correct folding of the aptamer domain, with the third model retaining only P3 and P4 (Fig. 5B, right). Interestingly, in all three models, the nonnative 5′ terminal G nucleotides, included in the sequence as a consequence of T7 RNA polymerase-based synthesis, are predicted to be involved in base pairs. These 5′ Gs are paired with either highly reactive nucleotides or nucleotides that form

very small duplexes (3 nt), however may still represent true members of the measured ensemble. Pairing probability arc plots for both the SreA aptamer and full-length SreA riboswitch were generated based on Switch-MaP reactivities (Fig. 5C). Manual alignment of the pairing probability plots, anchored by the aptamer domain, revealed agreement between the models, including well-determined P1-4 helices. Switch-MaP-derived pairing probabilities of the full-length SreA riboswitch supported terminator stem formation in the expression platform, which is in contrast to the primer- (Fig. 3) or structure cassette-derived MaP structures (Fig. 4), which favored the antiterminator or misfolded expression platform, respectively.

Structure modeling relies on critical nucleotide reactivities

To highlight the importance of retaining reactivity data for each nucleotide in the RNA, we simulated primer masking of the SreA aptamer using our Switch-MaP data (Fig. 6). We modeled the secondary structure of the SreA aptamer excluding reactivity data for 5′ and 3′ regions where cDNA amplification primers would otherwise anneal in a primer-based experiment. When reactivity data for both primer regions were omitted (−2 to 15 and 99 to +2), the minimum free energy model included perturbed P2, P3, and J3/4 elements (Supplemental Fig. S6), similar to our experimentally derived primer-MaP data (Supplemental Fig. 2). We next sequentially reduced the length of the 5′ masked region to determine which reactivities were critical for proper modeling (Supplemental Fig. S6). We discovered that the inclusion of reactivity data for G13, at the base of the P2 stem, was sufficient to restore the correct structure in the minimum free energy model (Fig. 6, compare left to center), and that no further masked region shortening had any impact on modeling (Fig. 6, right). Interestingly, simulated 3′ primer masking alone did not influence modeling of the aptamer fold. Therefore, it is difficult to predict how few or how many nucleotides will have a significant impact on modeling outcomes, underlining the importance of obtaining as complete a set of reactivity data as possible.

DISCUSSION

In contrast to traditional primer-based and cassette-based structure mapping techniques, Switch-MaP eliminates primer masking artifacts and precludes observation of non-native RNA secondary structures. Additionally, traditional MaP techniques can be problematic for novel RNA targets which lack structural characterization or known homology that inform the design of primers and/or noninterfering structure cassettes. Therefore, Switch-MaP may be appropriate for the characterization of novel RNAs, for which full coverage of the native sequence is imperative. Switch-MaP also represents a streamlined workflow, combining the addition of 5′ flanking sequences in the MaP RT itself. Any laboratory capable of MaP will be able to rapidly integrate Switch-MaP into their workflows.

Two additional extensions of Switch-MaP are clear: (1) application to any MaP-based approach, including those that measure RNA structure ensembles (Tomezsko et al. 2020; Morandi et al. 2021; Olson et al. 2022) or RNA–protein interactions (Weidmann et al. 2021), and (2) chemical probing of RNAs inside cells. Application to other chemical probing methods is straightforward: RNA probed with

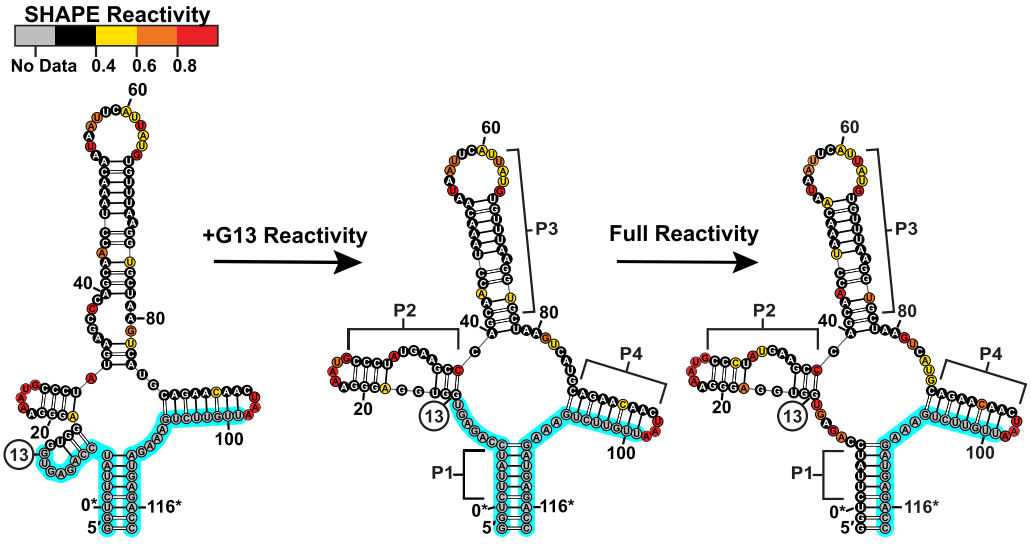

FIGURE 6. Simulated primer masking demonstrates critical nucleotide reactivities. Secondary structure predictions based on exclusion of experimental Switch-MaP reactivities for nt −2 to 13 and 99 to +2 (indicated by blue highlight) of the SreA aptamer construct (*left*). Restoration of G13 reactivity generated the expected aptamer fold (*center*) and is equivalent to structural prediction encompassing full reactivity data for 5′ end (*right*).

any chemical reagent can be used as a template for Switch-MaP library preparation, including RNA that was probed inside cells. Indeed, dual ligation approaches have successfully been applied to generate full-length probing data for tRNAs inside cells (tRNA structure-seq) (Yamagami et al. 2022), and substitution of secondary ligation with template-switching MaP would be a straightforward way to reduce preparative steps in similar approaches. In summary, Switch-MaP represents a straightforward approach for more complete analysis of RNA chemical probing data, and we expect the technology to be widely adopted for its ease of use and modularity with existing workflows.

MATERIALS AND METHODS

Construct design

The sequence of full-length SreA was identified from the *L. monocytogenes* EGD-e genome (Loh et al. 2009; Toledo-Arana et al. 2009). A gene block for full-length SreA was ordered from Integrated DNA Technologies (IDT) and contained the full-length riboswitch sequence, a T7 promoter, a 5′ hammer head (HH) ribozyme, and flanking restriction sites (Supplemental Table S2). The *SreA* gene block was restriction digested and cloned into the pUC57 plasmid. The conserved aptamer domain of *SreA* was identified by secondary structure prediction using the Dynalign algorithm from RNAstructure (Reuter and Mathews 2010). RNA sequences for SreA and the *B. subtilis yitJ* SAM-I riboswitch sequence were included in Dynalign structure prediction to help model a SAM-I riboswitch-like secondary structure (Supplemental Table S3; Grundy and Henkin 1998). Cassette constructs were generated via Overlap Extension PCR in a three-step assembly with gel purification to append the cassette sequences to the 5′ and 3′ position of both the full-length SreA and SreA aptamer constructs (Supplemental Table S2).

PCR amplification of DNA templates for T7 RNA polymerase

DNA templates for full-length, aptamer domain and cassette SreA constructs were generated by PCR amplification of SreA pUC57 plasmid with EconoTaq PLUS 2× Master Mix (Lucigen) and various primers (Supplemental Table S4). For a full-length SreA template, primers were complementary to a pUC57 sequence upstream of the transcription start site and to the 3′ end of the full-length riboswitch sequence (Supplemental Table S4). For the SreA aptamer domain, primers were complementary to the 5′ and 3′ ends of the P1 stems identified during structure prediction (Supplemental Table S4): The forward primer included a 5′ T7 RNAP promoter sequence followed by two G residues to facilitate transcription initiation with T7 RNAP, and the reverse primer contained two 5′ C residues meant to base-pair with the additional G residues. These primers' result is the addition of two nonnative G-C base pairs at the base of the P1 stem. Reverse primers for full-length and aptamer domain PCR strategies contained two 2′-*O*-methyl residues on the 5′ end to help limit nontemplated transcription (Kao et al. 1999).

RNA synthesis with T7 RNA polymerase

RNA was prepared by in vitro transcription using established methods (Zhang et al. 2020). Transcription reactions were performed in T7 transcription buffer (40 mM Tris-base pH 8.5, 5 mM DTT, 1 mM spermidine, 0.01% Triton-X) with T7 RNA polymerase (prepared in house). The transcription reaction included 3–6 mM rNTPs, 10–20 mM $MgCl_2$, 30–40 ng/µL DNA template, 0.2 U/mL yeast inorganic pyrophosphatase, ∼15 µM T7 RNA polymerase, and 10%–20% (vol/vol) DMSO (Helmling et al. 2015). The reactions were incubated at 37°C for 3–4 h and were quenched using a solution of 7 M urea and 250 mM EDTA (pH 8.5). RNA was purified from the reaction mixture by preparative scale denaturing polyacrylamide gel electrophoresis (PAGE). The target RNA was UV shadowed, excised, and electroeluted from the gel in TBE gel elution buffer (44.5 mM Tris-base, 44.5 mM boric acid, 5.0 mM EDTA, pH 8.3). The RNA was spin-concentrated, salt-washed with 2 M ultrapure NaCl, and exchanged into water using 10 kDa molecular weight cut-off Amicon Centrifugal Filter Units (MilliporeSigma).

Acylation of RNA for Switch-MaP and primer-based SHAPE-MaP

Riboswitch RNA at a concentration of 71.4 nM was denatured by heating to 95°C for 3 min and cooling on ice for 3 min. Denatured RNA was added to folding buffer at a 1.1× buffer concentration (110 mM HEPES pH 8.0, 110 mM NaCl, 5.5 mM $MgCl_2$) and was incubated for 20 min on 37°C heat block. The RNA sample was divided into two equal volume aliquots. While incubating on a 37°C heat block, one aliquot was added to 1/10th volume of anhydrous DMSO, and the second aliquot was added to 1/10th volume of 100 mM 11M7 prepared in anhydrous DMSO, resulting in 1× folding buffer reactions (100 mM HEPES pH 8.0, 100 mM NaCl, 5 mM $MgCl_2$), with 1.4 mM DMSO and 10 mM 1M7 in the treated sample. The samples were incubated for 2 min (in excess of the 17 sec aqueous half-life of 1M7) at 37°C and 250 rpm on the heat block (Busan et al. 2019). The RNA samples were exchanged into water using 10 kDa molecular weight cut-off Amicon Centrifugal Filter Units. This procedure was applied successfully to a range of RNA starting amounts between 10 and 1000 pmol.

Primer-masked MaP RT

MaP RT of the full-length SreA construct was performed largely as previously described. In 10 µL of total volume, 5 pmol of modified RNA was denatured at 70°C for 5 min in a mixture containing 20 nmol of each dNTP base and an RT primer complementary to the 3′ end of the RNA (Supplemental Table S4). After 5 min, the mixture was immediately placed at 4°C for 2 min. Nine microliters of freshly made 2.22× MaP buffer (111 mM Tris-HCl [pH 8.0], 167 mM KCl, 13.3 mM $MnCl_2$, 22 mM DTT, and 2.22 M betaine) was added to the mixture, which was then equilibrated at 25°C for 2 min. Subsequently, 1 µL (200 units) of SSIIRT (Invitrogen) was added to the reaction, which was then placed in a thermocycler with the following settings: 10 min at 25°C, 90 min at 42°C, 10 cycles of 2 min at 42°C and 2 min at 50°C, and finally 10 min at 70°C to heat inactivate the SSIIRT.

Ligation of preadenylated DNA adapter to SHAPE-modified aptamer domain and full-length RNA

In total, 20 pmol of purified aptamer domain RNA was ligated to 40 pmol of the 3′ preadenylated DNA adapter (Supplemental Table S1) at 25°C for 2 h in a reaction mixture containing 10% DMSO, 25% PEG 8000, 10 U T4 RNA ligase 1 (NEB), 50 mM Tris-HCl pH 7.5, 10 mM $MgCl_2$, and 1 mM DTT. RNA was purified from the ligation reaction using the RNA Clean and Concentrator-5 Kit (Zymo) and eluted in 20 µL of water. Ligation products were verified with a high-sensitivity RNA ScreenTape on a 4150 TapeStation System (Agilent) (Supplemental Fig. S1). For the full-length SreA riboswitch, purification proceeded using the RNA Clean and Concentrator-5 kit (Zymo) using the size selection protocol to remove excess 3′ preadenylated DNA adaptor.

Guanosine capping of aptamer domain RNA

To promote template switching during RT, the Vaccinia Capping System (NEB) was used without SAM to add a G_{cap} structure to the 5′ end of the adapter ligated RNA templates. Twenty microliters of adapter ligated RNA was denatured at 65°C for 5 min and cooled on ice for 5 min. The adapter ligated RNA was subsequently incubated at 37°C for 30 min in a reaction containing 0.5 mM GTP and 0.5 U/µL vaccinia capping enzyme and capping buffer (50 mM Tris-HCl pH 8, 5 mM KCl, 1 mM $MgCl_2$, 1 mM DTT).

Map RT with template switching oligonucleotide (Switch-MaP)

To collect SHAPE reactivity information at the 5′ end of the SreA aptamer domain RNA, we included a TSO (Supplemental Table S1) in a MaP-RT reaction. Switch-MaP-RT reactions were carried out on G-capped RNA under the same reaction conditions as the primer-based MaP RT reactions, except for the addition of 100 pmol of TSO to the template solution and an RT primer complementary to the ligated 3′ adapter (Supplemental Table S1). Incorporation of the TSO complementary sequence in the cDNA product was verified with a high-sensitivity DNA ScreenTape on a 4150 TapeStation System (Supplemental Fig. S2). For the full-length SreA construct, unincorporated TSO was removed via the RNA Clean and Concentrator-5 kit (Zymo) using the size selection protocol.

Library preparation and sequencing

Targeted amplicon sequencing libraries were generated by PCR. One microliter of cDNA from the MaP-RT reaction was used as a template for PCR with 5 µL each of 5 µM i5/i7 indexing primers (Supplemental Table S4) and Q5 hot-start polymerase (NEB) in a total reaction volume of 50 µL. The reactions were performed in a thermocycler with the following conditions: 30 sec at 98°C, 15 × (10 sec at 98°C, 30 sec at 67°C and 30 sec at 72°C), and 2 min at 72°C. PCR products were purified with 1× volume of SPRI beads, beads were washed twice with 80% ethanol, and libraries were eluted with 15 µL of nuclease-free water. Size distributions and purities of amplicon libraries were verified (4150 TapeStation, Agilent). About 120 pmol of each library was sequenced on a MiSeq instrument (Illumina) with 2× 150 paired-end sequencing.

Analysis with ShapeMapper2 and RNAStructure

FASTQ files from sequencing runs were input into ShapeMapper2 for read alignment to the SreA sequence and mutation counting (Busan and Weeks 2018). ShapeMapper2 defaults were used, other than the –min-depth FLAG, which was reduced to 4000. Normalized reactivity values from ".shape' outputs generated by Shapemapper2 were used for downstream structural modeling. Models of RNA secondary structures were generated from normalized SHAPE reactivities using RNAstructure Fold with default folding parameters and the -sh FLAG (Reuter and Mathews 2010; Busan and Weeks 2018). Partition function calculations were performed using RNAStructure partition with the -sh FLAG when including .shape information. Pairing probability dot plot text files were created using RNAStructure utility ProbabilityPlot and the partition .pfs output with the -t FLAG. Pairing probability arc plots were generated from probability dot plots, .shape reactivity files, and the arcPlot.py software (available at https://github.com/Weeks-UNC/arcPlot).

DATA DEPOSITION

Raw sequencing data and intermediate processed files are available through the Gene Expression Omnibus (GEO) with accession number GSE274121.

SUPPLEMENTAL MATERIAL

Supplemental material is available for this article.

ACKNOWLEDGMENTS

We acknowledge the funding support from the National Science Foundation (MCB-1942398 to S.C.K.). C.A.W. is supported by an NCI transition award (K22CA262349), startup funds from the University of Michigan Center for RNA Biomedicine, and an NCI Support Grant for the Rogel Cancer Center (P30CA046592).

Received December 13, 2023; accepted September 26, 2024.

REFERENCES

Assmann S, Chou H, Bevilacqua P. 2023. Rock, scissors, paper: how RNA structure informs function. *Plant Cell* **35:** 1671–1707. doi:10.1093/plcell/koad026

Batey RT. 2011. Recognition of *S*-adenosylmethionine by riboswitches. *WIREs RNA* **2:** 299–311. doi:10.1002/wrna.63

Busan S, Weeks KM. 2018. Accurate detection of chemical modifications in RNA by mutational profiling (MaP) with ShapeMapper 2. *RNA* **24:** 143–148. doi:10.1261/rna.061945.117

Busan S, Weidmann CA, Sengupta A, Weeks KM. 2019. Guidelines for SHAPE reagent choice and detection strategy for RNA structure probing studies. *Biochemistry* 2019, **58:** 2655–2664. doi:10.1021/acs.biochem.8b01218

Cech TR, Steitz JA. 2014. The noncoding RNA revolution-trashing old rules to forge new ones. *Cell* **157:** 77–94. doi:10.1016/j.cell.2014.03.008

Christy TW, Giannetti CA, Houlihan G, Smola MJ, Rice GM, Wang J, Dokholyan N V, Laederach A, Holliger P, Weeks KM. 2021.

Direct mapping of higher-order RNA interactions by SHAPE-JuMP. *Biochemistry* **60:** 1971–1982. doi:10.1021/acs.biochem.1c00270

Dann CE, Wakeman CA, Sieling CL, Baker SC, Irnov I, Winkler WC. 2007. Structure and mechanism of a metal-sensing regulatory RNA. *Cell* **130:** 878–892. doi:10.1016/j.cell.2007.06.051

Deigan KE, Li TW, Matthews DH, Weeks KM. 2009. Accurate SHAPE-directed RNA structure determination. *Proc Natl Acad Sci* **106:** 97–102. doi:10.1073/pnas.080692910

Dethoff EA, Boerneke MA, Gokhale NS, Muhire BM, Martin DP, Sacco MT, McFadden MJ, Weinstein JB, Messer WB, Horner SM, et al. 2018. Pervasive tertiary structure in the dengue virus RNA genome. *Proc Natl Acad Sci* **115:** 11513–11518. doi:10.1073/pnas.1716689115

Eddy SR. 2001. Non-coding RNA genes and the modern RNA world. *Nat Rev Genet* **2:** 919–929. doi:10.1038/35103511

Edwards TE, Ferré-D'Amaré AR. 2006. Crystal structures of the *thi*-box riboswitch bound to thiamine pyrophosphate analogs reveal adaptive RNA-small molecule recognition. *Structure* **14:** 1459–1468. doi:10.1016/j.str.2006.07.008

Fuchs RT, Grundy FJ, Henkin TM. 2006. The SMK box is a new SAM-binding RNA for translational regulation of SAM synthetase. *Nat Struct Mol Biol* **13:** 226–233. doi:10.1038/nsmb1059

Garst AD, Héroux A, Rambo RP, Batey RT. 2008. Crystal structure of the lysine riboswitch regulatory mRNA element. *J Biol Chem* **283:** 22347–22351. doi:10.1074/jbc.C800120200

Grundy FJ, Henkin TM. 1998. The S box regulon: a new global transcription termination control system for methionine and cysteine biosynthesis genes in Gram-positive bacteria. *Mol Microbiol* **30:** 737–749. doi:10.1046/j.1365-2958.1998.01105.x

Hajdin CE, Bellaousov S, Huggins W, Weeks KM. 2013. SHAPE-directed RNA secondary structure modeling, including pseudoknots. *Proc Natl Acad Sci* **110:** 5498–5503. doi:10.1073/pnas.1219988110

Helmling C, Keyhani S, Sochor F, Fürtig B, Hengesbach M, Schwalbe H. 2015. Rapid NMR screening of RNA secondary structure and binding. *J Biomol NMR* **63:** 67–76. doi:10.1007/s10858-015-9967-y

Kao C, Zheng M, Rüdisser S. 1999. A simple and efficient method to reduce nontemplated nucleotide addition at the 3′ terminus of RNAs transcribed by T7 RNA polymerase. *RNA* **5:** 1268–1272. doi:10.1017/S1355838299991033

Kawano M, Reynolds AA, Miranda-Rios J, Storz G. 2005. Detection of 5′- and 3′-UTR-derived small RNAs and *cis*-encoded antisense RNAs in *Escherichia coli*. *Nucleic Acids Res* **33:** 1040–1050. doi:10.1093/nar/gki256

Lagos-Quintana M, Rauhut R, Lendeckel W, Tuschl T. 2001. Identification of novel genes coding for small expressed RNAs. *Science* **294:** 853–858. doi:10.1126/science.1064921

Lau NC, Lim LP, Weinstein EG, Bartel DP. 2001. An abundant class of tiny RNAs with probable regulatory roles in *Caenorhabditis elegans*. *Science* **294:** 858–862. doi:10.1126/science.1065062

Lee RC, Ambros V. 2001. An extensive class of small RNAs in *Caenorhabditis elegans*. *Science* **294:** 862–864. doi:10.1126/science.1065329

Loh E, Dussurget O, Gripenland J, Vaitkevicius K, Tiensuu T, Mandin P, Repoila F, Buchrieser C, Cossart P, Johansson J. 2009. A *trans*-acting riboswitch controls expression of the virulence regulator PrfA in *Listeria monocytogenes*. *Cell* **139:** 770–779. doi:10.1016/j.cell.2009.08.046

Loughrey D, Watters KE, Settle AH, Lucks JB. 2014. SHAPE-Seq 2.0: systematic optimization and extension of high-throughput chemical probing of RNA secondary structure with next generation sequencing. *Nucleic Acids Res* **42:** e165. doi:10.1093/nar/gku909

Lu C, Ding F, Chowdhury A, Pradhan V, Tomsic J, Holmes WM, Henkin TM, Ke A. 2010. SAM recognition and conformational switching mechanism in the *Bacillus subtilis yitJ* S Box/SAM-I riboswitch. *J Mol Biol* **404:** 803–818. doi:10.1016/j.jmb.2010.09.059

Maguire S, Lohman G, Guan S. 2020. A low-bias and sensitive small RNA library preparation method using randomized splint ligation. *Nucleic Acids Res* **48:** e80. doi:10.1093/nar/gkaa480

Mathews DH. 2004. Using an RNA secondary structure partition function to determine confidence in base pairs predicted by free energy minimization. *RNA* **10:** 1178–90. doi: 10.1261/rna.7650904

Mattick JS, Makunin IV. 2006. Non-coding RNA. *Hum Mol Genet* **15:** R17–R29. doi:10.1093/hmg/ddl046

Mattick JS, Amaral PP, Carninci P, Carpenter S, Chang HY, Chen LL, Chen R, Dean C, Dinger ME, Fitzgerald KA, et al. 2023. Long non-coding RNAs: definitions, functions, challenges and recommendations. *Nat Rev Mol Cell Biol* **24:** 430–447. doi:10.1038/s41580-022-00566-8

McDaniel BA, Grundy FJ, Henkin TM. 2005. A tertiary structural element in S box leader RNAs is required for *S*-adenosylmethionine-directed transcription termination. *Mol Microbiol* **57:** 1008–1021. doi:10.1111/j.1365-2958.2005.04740.x

Merino EJ, Wilkinson KA, Coughlan JL, Weeks KM. 2005. RNA structure analysis at single nucleotide resolution by Selective 2′-Hydroxyl Acylation and Primer Extension (SHAPE). *J Am Chem Soc* **127:** 4223–4231. doi:10.1021/ja043822v

Montange RK, Batey RT. 2006. Structure of the *S*-adenosylmethionine riboswitch regulatory mRNA element. *Nature* **441:** 1172–1175. doi:10.1038/nature04819

Montange RK, Mondragón E, van Tyne D, Garst AD, Ceres P, Batey RT. 2010. Discrimination between closely related cellular metabolites by the SAM-I riboswitch. *J Mol Biol* **396:** 761–772. doi:10.1016/j.jmb.2009.12.007

Morandi E, Manfredonia I, Simon LM, Anselmi F, van Hemert MJ, Oliviero S, Incarnato D. 2021. Genome-scale deconvolution of RNA structure ensembles. *Nat Methods* **18:** 249–252. doi:10.1038/s41592-021-01075-w

Olson SW, Turner A-MW, Arney JW, Saleem I, Weidmann CA, Margolis DM, Weeks KM, Mustoe AM. 2022. Discovery of a large-scale, cell-state-responsive allosteric switch in the 7SK RNA using DANCE-MaP. *Mol Cell* **82:** 1708–1723.e10. doi:10.1016/j.molcel.2022.02.009

Przanowska R, Weidmann C, Saha S, Cichewicz M, Jensen K, Przanowski P, Irving P, Janes K, Guertin M, Weeks K. 2022. Distinct *MUNC* lncRNA structural domains regulate transcription of different promyogenic factors. *Cell Rep* **38:** 110361. doi:10.1016/j.celrep.2022.110361

Reinhart BJ, Slack FJ, Basson M, Pasquinelli AE, Bettinger JC, Rougvie AE, Horvitz HR, Ruvkun G. 2000. The 21-nucleotide *let-7* RNA regulates developmental timing in *Caenorhabditis elegans*. *Nature* **403:** 901–906. doi:10.1038/35002607

Reuter JS, Mathews DH. 2010. RNAstructure: software for RNA secondary structure prediction and analysis. *BMC Bioinfor* **11:** 129 doi:10.1186/1471-2105-11-129

Santosh B, Varshney A, Yadava PK. 2014. Non-coding RNAs: biological functions and applications. *Cell Biochem Function* **33:** 14–22. doi:10.1002/cbf.3079

Siegfried NA, Busan S, Rice GM, Nelson JAE, Weeks KM. 2014. RNA motif discovery by SHAPE and mutational profiling (SHAPE-MaP). *Nat Methods* **11:** 959–965. doi:10.1038/nmeth.3029

Stoddard CD, Montange RK, Hennelly SP, Rambo RP, Sanbonmatsu KY, Batey RT. 2010. Free state conformational sampling of the SAM-I riboswitch aptamer domain. *Structure* **18:** 787–797. doi:10.1016/2Fj.str.2010.04.006

Schroeder KT, Daldrop P, Lilley DMJ. 2011. RNA tertiary interactions in a riboswitch stabilize the structure of a kink turn. *Structure* **19:** 1233–1240. doi:10.1016/2Fj.str.2011.07.003

Thore S, Leibundgut M, Ban N. 2006. Structure of the eukaryotic thiamine pyrophosphate riboswitch with its regulatory ligand. *Science* **312:** 1208–1211. doi:10.1126/science.1128451

Tian D, Sun S, Lee JT. 2010. The long noncoding RNA, Jpx, is a molecular switch for X chromosome inactivation. *Cell* **143:** 390–403. doi:10.1016/j.cell.2010.09.049

Toledo-Arana A, Dussurget O, Nikitas G, Sesto N, Guet-Revillet H, Balestrino D, Loh E, Gripenland J, Tiensuu T, Vaitkevicius K, et al. 2009. The Listeria transcriptional landscape from saprophytism to virulence. *Nature* **459:** 950–956. doi:10.1038/nature08080

Tomezsko PJ, Corbin VDA, Gupta P, Swaminathan H, Glasgow M, Persad S, Edwards MD, Mcintosh L, Papenfuss AT, Emery A, et al. 2020. Determination of RNA structural diversity and its role in HIV-1 RNA splicing. *Nature* **582:** 438–442. doi:10.1038/s41586-020-2253-5

Vogel J, Bartels V, Tang TH, Churakov G, Slagter-Jäger JG, Hüttenhofer A, Wagner EGH. 2003. RNomics in *Escherichia coli* detects new sRNA species and indicates parallel transcriptional output in bacteria. *Nucleic Acids Res* **31:** 6435–6443. doi:10.1093/nar/gkg867

Wassarman KM, Repoila F, Rosenow C, Storz G, Gottesman S. 2001. Identification of novel small RNAs using comparative genomics and microarrays. *Genes Dev* **15:** 1637–1651. doi:10.1101/gad.901001

Weidmann CA, Mustoe AM, Jariwala PB, Calabrese JM, Weeks KM. 2021. Analysis of RNA–protein networks with RNP-MaP defines functional hubs on RNA. *Nat Biotechnol* **39:** 347–356. doi:10.1038/s41587-020-0709-7

Wilkinson KA, Merino EJ, Weeks KM. 2006. Selective 2′-hydroxyl acylation analyzed by primer extension (SHAPE): quantitative RNA structure analysis at single nucleotide resolution. *Nat Protoc* **1:** 1610–1616. doi:10.1038/nprot.2006.249

Winkler WC, Nahvi A, Sudarsan N, Barrick JE, Breaker RR. 2003. An mRNA structure that controls gene expression by binding *S*-adenosylmethionine. *Nat Struct Biol* **10:** 701–707. doi:10.1038/nsb967

Wulf MG, Maguire S, Dai N, Blondel A, Posfai D, Krishnan K, Sun Z, Guan S, Corrêa IR Jr. 2022. Chemical capping improves template switching and enhances sequencing of small RNAs. *Nucleic Acids Res* **50:** e2. doi:10.1093/nar/gkab861

Yamagami R, Sieg JP, Assmann SM, Bevilacqua PC. 2022. Genome-wide analysis of the in vivo tRNA structurome reveals RNA structural and modification dynamics under heat stress. *Proc Natl Acad Sci* **119:** e2201237119. doi:10.1073/pnas.2201237119

Zhang H, Hall I, Nissley AJ, Abdallah K, Keane SC. 2020. A tale of two transitions: the unfolding mechanism of the prfA RNA thermosensor. *Biochemistry* **59:** 4533–4545. doi:10.1021/acs.biochem.0c00588

Zhu Y, Machleder E, Chenchik A, Li R, Siebert P. 2001. Reverse transcriptase template switching: a SMART™ approach for full-length cDNA library construction. *BioTechniques* **30:** 892–897. doi:10.2144/01304pf02

MEET THE FIRST AUTHORS

Martin O'Steen

***Meet the First Author(s)* is an editorial feature within *RNA*, in which the first author(s) of research-based papers in each issue have the opportunity to introduce themselves and their work to readers of *RNA* and the RNA research community. Martin O'Steen is co-first author of this paper, "Template switching enables chemical probing of native RNA structures," along with Ian Hall. Martin is a research fellow in biophysics at the College of Literature, Science, and the Arts, University of Michigan, in the lab of Sarah Keane. Martin's research focuses on elucidating the structure–function relationship of noncoding RNA.**

What are the major results described in your paper and how do they impact this branch of the field?

We developed a new ligation approach for RNA chemical probing experiments. This method allows full capture of nucleotide reactivities, providing a more accurate predication of the RNA of interest. As shown in our work, these predictions are sensitive, with the loss of a single reactivity generating improper structures.

What led you to study RNA or this aspect of RNA science?

Both Dr. Ian Hall and I were interested in furthering the field of chemical probing experiments. This new approach allows for more accurate structure generation.

If you were able to give one piece of advice to your younger self, what would that be?

MO: That science is often difficult and frustrating. The key to good science is perseverance and creativity. Foster both of those and the rest will fall in place.

What are your subsequent near- or long-term career plans?

MO: I would like to continue my training as a research fellow in RNA structural science in the immediate future. Following this, I would like to pursue a career in academia studying natural RNA motifs from a structural perspective, to identify aspects/strategies of these natural RNAs that can be applied to artificial functional sequences, such as aptamers and ribozymes, to improve their function in a biological context.

What were the strongest aspects of your collaboration as co-first authors?

Dr. Ian Hall was a fabulous collaborator. I would say his strongest aspect was strong communication skills, allowing us to benefit from each other's ideas.

Template switching enables chemical probing of native RNA structures

Ian Hall, Martin O'Steen, Sophie Gold, et al.

RNA 2025 31: 113-125 originally published online October 22, 2024
Access the most recent version at doi:10.1261/rna.079926.123